Optics Letters

All-optical dispersive Fourier analysis for ultrafast user localization at 50 MHz in beam-steered optical wireless communication

Yuanli Yue,[1] Yue Feng,[1,2] Shouju Liu,[1] and Chao Wang[1,*]

[1]School of Engineering Mathematics and Physics, University of Kent, Canterbury, CT2 7NZ, UK
[2]School of Measurement and Control Technology and Communication Engineering, Harbin University of Science and Technology, 150080, Harbin, China
*c.wang@kent.ac.uk

Received 19 September 2025; revised 16 October 2025; accepted 20 October 2025; posted 27 October 2025; published 21 November 2025

Beam-steered optical wireless communication (OWC) enables high-capacity indoor links where real-time user localization is crucial. We propose and experimentally demonstrate an all-optical method for ultrafast localization operating at 50 MHz in wavelength-controlled beam-steered OWC. The scheme exploits the mapping between user position and the wavelength of retro-reflected signals. Instantaneous wavelength identification is achieved through all-optical frequency coding and dispersive Fourier transform (DFT), allowing user positions to be derived from the time interval between two optical pulses without high-speed detection or digital processing. A theoretical model confirms a linear relation between instantaneous frequency and pulse interval, validated by numerical and experimental results. By shifting Fourier analysis entirely into the optical domain, the method offers a simple, low-cost, and energy-efficient solution for real-time and ultrafast user-specific localization in beam-steered OWC systems.

https://doi.org/10.1364/OL.579591

Optical wireless communication (OWC) has emerged as a promising solution to the growing demand for wireless bandwidth [1]. With a license-free optical spectrum and broad frequency range [2,3], it is well suited for high-speed indoor communications. While the Global Positioning System (GPS) dominates outdoor localization [4], its accuracy deteriorates indoors due to structural obstructions, making efficient indoor localization a key research focus.

Beam-steered OWC enables targeted data delivery to users via visible light (VLC) or infrared (BS-ILC) links [5]. VLC leverages existing LEDs but suffers from limited bandwidth and ambient light interference, whereas beam steering achieves higher efficiency using independent optical channels. Passive diffractive elements such as fiber Bragg gratings (TFBGs) enable wavelength-dependent routing without electrical control, allowing faster and simpler operation than active devices [3].

Various indoor localization methods—such as Wi-Fi, ZigBee, algorithmic, and Short-Time Fourier Transform (STFT)-based approaches—have been explored [6], but they suffer from high latency and energy consumption, limiting real-time performance. A key challenge in beam-steered OWC is real-time tracking of mobile user terminals. Our previous work showed that wavelength-controlled beam-steered OWC enables ultrafast localization by identifying the instantaneous microwave frequency of the optical carrier [7]. Although reservoir computing improves accuracy, it introduces significant computational overhead. Balancing accuracy and real-time operation remains a major challenge.

In this Letter, we propose a novel scheme for real-time user localization in wavelength-controlled beam-steered OWC using an all-optical dispersive Fourier transform (FT). This work is an extension of our previously reported study on reservoir computing–assisted ultrafast localization in beam-steering optical wireless systems [7]. In that earlier work, both angular and linear distance information were extracted simultaneously based on the wavelength–angle mapping of a 45° TFBG and the optical time-of-flight delay. This Letter focuses on developing a new all-optical implementation of the same localization principle by employing dispersive pulse compression to identify the carrier frequency directly in the optical domain. Unlike digital STFT-based methods, our approach uses dispersive fiber to perform analog Fourier analysis directly in the optical domain. The temporal separation of split sideband pulses enables precise frequency extraction for low-latency, energy-efficient user localization.

The proposed ultrafast user localization system (Fig. 1) consists of four modules: pulse time-stretching, chirp coding, beam steering, and data processing. Following the wavelength–angle and time-of-flight mapping principle in [7], this work emphasizes an all-optical frequency identification mechanism using pulse compression for real-time implementation. An ultrashort pulse emitted by a Mode-Locked Laser (MLL) is first temporally stretched and chirp-encoded using an unbalanced Mach–Zehnder interferometer (MZI), which performs the chirp-coding function and establishes a frequency–time mapping that links optical frequencies to distinct temporal

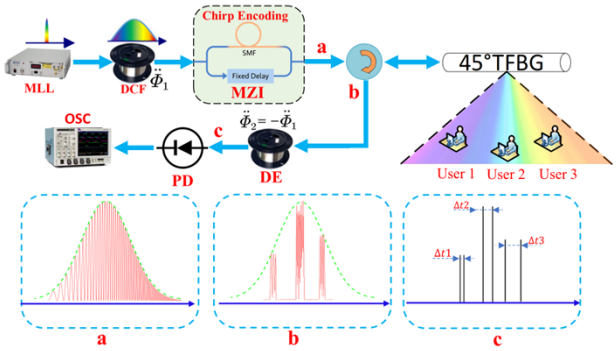

Fig. 1. The schematic of the proposed ultrafast user localization system.

positions. Ultrafast wavelength-controlled beam steering is subsequently realized using a 45° TFBG. A 45° TFBG then performs wavelength-controlled beam steering with an angular dispersion of 0.22°/nm, providing a 2.5° steering range over a 12-nm bandwidth. The steering speed, governed by the 50 MHz pulse rate, enables sub-microsecond updates. Because the wavelength–angle mapping is fixed, each user's reflection remains linked to its wavelength channel, allowing stable real-time tracking for optical wireless localization. Leveraging the TFBG's dispersive properties, different wavelengths carrying distinct microwave frequencies are directed toward corresponding users, enabling precise targeting of chirped signals based on the frequency–time mapping.

The reflected pulses from remote users are collected by the same 45° TFBG and coupled into a dispersion-compensating fiber (DCF), where opposite dispersion compresses them. Through dispersive FT, the pulses split into two components corresponding to the upper and lower microwave sidebands. These are detected by a Photodetector (PD) and recorded on a real-time oscilloscope (OSC). The central microwave frequency is determined from the temporal separation of the two pulses.

In the analysis, the third-order dispersion (TOD) of the dispersive elements (DEs) is assumed negligible [8], and only second-order dispersion (SOD) or group velocity dispersion (GVD) is considered. This assumption is justified since the TOD of the dispersive elements is much smaller than the SOD within the operating bandwidth. Hence, the impact of TOD on pulse stretching and compression can be safely neglected. An MLL serves as the light source, and the input power is kept low to suppress nonlinear effects in the DEs. The input optical pulse is modeled as a transform-limited Gaussian pulse, expressed as:

$$g(t) = \exp\left(-t^2/\tau_0^2\right), \tag{1}$$

where τ_0 is the half pulse-width at $1/e$ maximum. Its FT can be given by:

$$G(\omega) = \sqrt{\pi}\tau_0 \exp\left(-\tau_0\omega^2/4\right). \tag{2}$$

In this model, a DCF with dispersion coefficient Φ_1 is used for time-stretching. As the ultrashort optical pulse propagates through the DE, it is temporally broadened and spectrally mapped. The output optical signal is expressed as:

$$P(\omega) = G(\omega) \times \exp\left(j\ddot{\Phi}_1\omega^2/2\right). \tag{3}$$

To generate a frequency-chirped pulse, an unbalanced MZI with a single-mode fiber delay line in one arm is employed [9]. The transfer function of the unbalanced MZI can be expressed as:

$$H_2(\omega) = \frac{1}{2}\left[\exp\left(-j\omega t_1 + j\frac{\ddot{\Phi}_v}{2}\right) + \exp(-j\omega t_2)\right], \tag{4}$$

where t_1 and t_2 are the time delays in the two MZI arms, $\ddot{\Phi}_v = \frac{d^2\theta\omega^2}{d\omega^2}\Big|_{\omega=\omega_0}$ (ps^2) is the second-order dispersion coefficient, and $\Delta t_{MZI} = t_2 - t_1$ is the delay difference between the two arms of the unbalanced MZI. Since higher-order dispersion is small, only second-order dispersion is considered.

After chirp coding, a one-to-one wavelength–frequency mapping is established. The chirped pulse is steered by the 45° TFBG toward different users, which reflect the beams back to the same grating. These reflections are coupled into another DE for FT-based compression. Each user is assigned a unique optical path and wavelength corresponding to a specific steering angle, and the reflected field from the i-th user is modeled by a dispersive transfer function:

$$H_i(\omega) = \exp\left[\frac{-j\ddot{\Phi}_2(\omega-\omega_i)^2}{2}\right], \quad (i = 1, 2, 3, \ldots) \tag{5}$$

In Eq. (5), $H_i(\omega)$ denotes the dispersive response of the i-th user, where ω_i is the central angular frequency of its wavelength channel and $\ddot{\Phi}_{2,i}$ is the second-order dispersion of the return path. The term $(\omega - \omega_i)$ represents the frequency deviation causing temporal broadening. The reflected amplitude may differ among users due to varying reflectivity and propagation losses.

The output signal of a Photonic Time–Stretch (PTS) system, $s(t)$, is the convolution of the input optical signal with the FT of the intensity modulation function [10]:

$$s(t) = g(t) * E_{IM}(\omega)\,|_{\omega=t/\Delta\ddot{\Phi}_1}, \tag{6}$$

$$s(t) = S_0\left[g(t-\Delta t) + g(t+\Delta t)\right], \tag{7}$$

where $E_{IM}(\omega) = \Im\left[e_{IM}(t)\right]$ is the FT of $e_{IM}(t)$, $e_{IM}(t)$ denotes the optical field after intensity modulation, (*) denotes convolution, $S_0 = J_1(\beta)/|\ddot{\Phi}_1|$ is a time-independent constant, and $\Delta t = |\omega_m\ddot{\Phi}_1|$ is a time delay introduced by the balanced PTS process. According to the equation, two replicas of the input optical pulse with a time delay difference of $2\Delta t$ are generated at the PTS output, corresponding to the two first-order optical sidebands of the MZI biased to suppress the carrier and the even-order sidebands.

According to the original setting, the two DEs have the same but converse value. In fact, there will be a residual dispersion $r(t)$. It is obtained by propagating the signal $s(t)$ through the second subsystem.

The input and output signals are related by the temporal convolution $r(t) = s(t) \cdot h_\Delta(t)$, where $h_\Delta(t) = \Im^{-1}\left[H_\Delta(\omega)\right]$ is the impulse response of the residual DE, $H_\Delta(\omega)$ denotes the transfer function of the residual DE. If the dispersion of the residual DE satisfies the condition $|\Delta\ddot{\Phi}| > \tau_0^2/2\pi$, the spectra of the individual pulses $g(t-\Delta t)$ and $g(t+\Delta t)$ are mapped to the time domain as two transformed waveforms $(\Im[g(t-\Delta t)]|_{\omega=t/\Delta\ddot{\Phi}}$ and $\Im[g(t+\Delta t)]|_{\omega=t/\Delta\ddot{\Phi}}$ due to the dispersion-induced real-time FT.

Since the two transformed waveforms are time-delayed, the time delay difference Δt represents a corresponding frequency

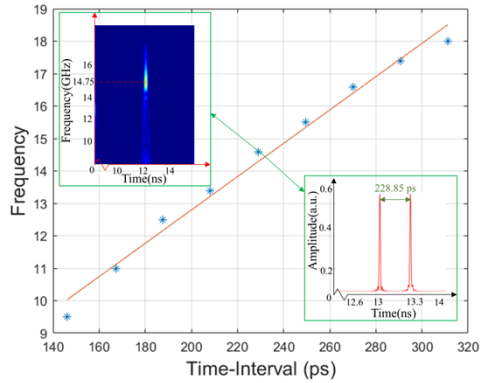

Fig. 2. The measured frequency–time difference mapping and its linear fitting result.

shear $\Delta\omega$ given by $\Delta\omega = \Delta t/\Delta\ddot{\Phi}$. based on the mapping relationship.

Numerical simulations and experiments were conducted to validate the proposed real-time indoor localization method. A passive MLL (50 MHz) generated 550 fs pulses that were stretched to 12 ns using a 25 km single-mode fiber for frequency-to-time mapping. Microwave frequencies from 7 GHz to 29 GHz were obtained within the stretched pulse window. The chirped puls were steered toward users via a 45° TFBG, establishing a frequency–time–space mapping. Each user received an optical pulse with a distinct central frequency within a 22 GHz bandwidth. Reflected pulses were recollected and compressed by a DCF, and the temporal separation between adjacent pulses on the OSC was used to determine the corresponding frequencies. In this framework, the reflected time delay and central frequency provide the information required for indoor localization. The wavelength-dependent delay is determined during the time-stretch process, while the actual time-of-flight corresponds to the user position. Combining these two factors yields the absolute user distance. In the simulation, four users were considered—one reference and three test users. Figure 2 shows the linear mapping between frequency and temporal separation in free space, yielding a slope of approximately 51.36 fs/GHz.

Determining the central frequency of each reflected pulse is essential for extracting user information. The STFT is commonly used for this purpose, providing reliable frequency estimation. In this work, we compare the performance of STFT with the proposed all-optical FT for independent central frequency detection. As shown in Fig. 2 (upper left), the STFT result for User 2 yields a central frequency of 14.5 GHz. In contrast, the optical FT approach determines the time interval between the two split pulses as 228.85 ps, corresponding to a central frequency of 14.6 GHz. The close agreement confirms the accuracy of our method and validates user localization.

To further verify the approach, a proof-of-concept experiment was conducted using a 50 MHz passive mode-locked fiber laser (Calmar Mendocino FP) generating 800 fs pulses with a 12 nm spectrum. The pulses were stretched to 12 ns by a DCF (–1.04 ns/nm), then amplified and chirp-encoded via an MZI with an optical delay line (VDL001) and 500 m SMF. Dispersion imbalance and delay adjustment in the MZI produced a wideband chirped pulse with a tunable frequency offset. Increasing the fiber length enhanced the chirp rate. This setup generated a monotonic RF sweep mapped to both time and wavelength domains, establishing a stable wavelength–frequency mapping. The chirp slope was extracted from the spectrogram in Fig. 3.

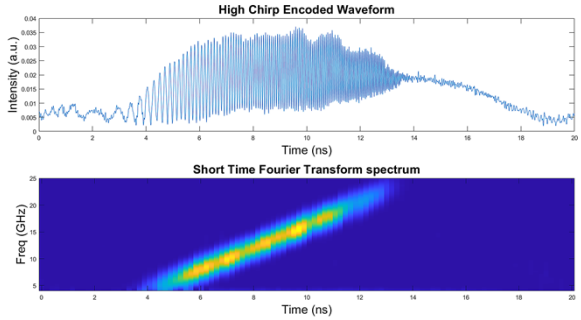

Fig. 3. High chirp encoded temporal domain waveform and corresponding spectrogram.

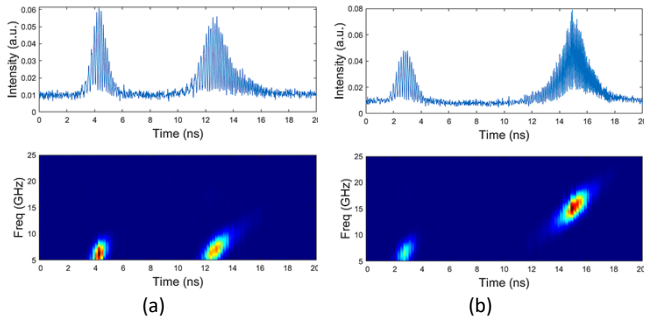

Fig. 4. The reflected pulses and the corresponding instantaneous microwave frequency measurement using STFT.

After chirp encoding and wavelength–time mapping are established, a fixed correspondence among wavelength, time, and RF frequency must be defined. A reference point can be obtained from a transmission window in the reflection profile, as shown in Fig. 3. To evaluate system performance, two groups of users were selected, as illustrated in Figs. 4(a) and 4(b). The reflected pulses were first analyzed using STFT to extract their central frequencies. For the left group, the central frequencies were 6.5 GHz and 6.9 GHz, while for the right group, they were 6.5 GHz and 15 GHz.

For further analysis, a 20-ns window was analyzed for both user groups. The reflected pulses were clearly detected, and their central frequencies were accurately identified by STFT. Using the first user (6.5 GHz) as a reference, the second user showed frequencies of 7.1 GHz and 15 GHz, enabling precise position estimation in free space.

To eliminate the need for frequency transformation via STFT, which is computationally intensive, we developed a novel approach based on optical pulse compression. In this work, a dispersion fiber with opposite dispersion compresses the echo signal, resulting in two split peaks whose temporal separation directly corresponds to the central frequency.

Experimentally, the compressed reflected pulses exhibited distinct time intervals, as shown in Fig. 5. For the first group, the measured intervals were approximately 60.4 ps and 53.6 ps, while for the second group, they were 61.4 ps and 135.2 ps. These results confirm that larger time intervals correspond to higher central frequencies. For example, a separation of 53.6 ps corresponds to 6.4 GHz, while 60.4 ps corresponds to 7.1 GHz,

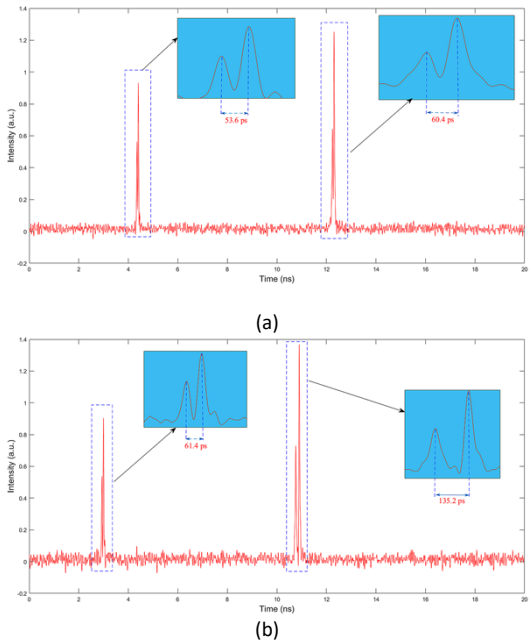

Fig. 5. The compressed output waveform due to optical FT.

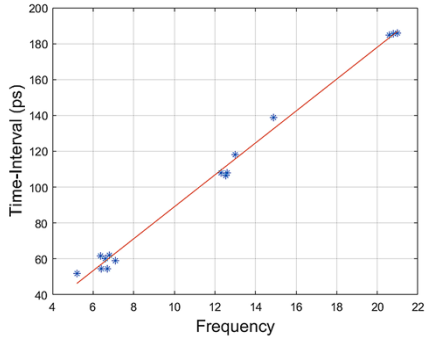

Fig. 6. The experimental frequency-to-time-interval mapping (blue-dotted) and its linear fitting result (red line).

demonstrating accurate frequency-to-time mapping for user localization.

Reflected pulse amplitudes vary among users due to variations in reflectivity, propagation loss, and coupling efficiency. Although not included in Eq. (5), these differences appear in the measured waveforms (Figs. 4 and 5), enabling user distinction by both delay and amplitude.

Additional experiments confirmed a linear relationship between time interval and central frequency, with a fitted slope of 8.9 ps/GHz, as shown in Fig. 6. With this mapping, user positions can be determined in real time from the time interval of the compressed pulses. This approach offers a reliable and efficient method for real-time indoor localization. Although a full two-dimensional localization test is not repeated here, the same wavelength–angle and distance retrieval principle from [7] applies. This work demonstrates that the optical pulse compression module accurately recovers the carrier frequency and integrates seamlessly into the established beam-steered OWC localization framework.

The measured frequency–time slope (8.9 ps/GHz) is much larger than the simulated value (51.36 fs/GHz) due to residual dispersion in the experimental setup. Unlike ideal compensation in simulation, dispersion from fibers, the TFBG, and other components accumulates in practice. This residual dispersion, on the order of hundreds of ps/nm, together with higher-order effects and detector bandwidth limits, accounts for the observed difference.

In conclusion, we experimentally demonstrated an all-optical DFT for real-time user localization in a wavelength-controlled beam-steered OWC system. A high-efficiency 45° tilted fiber grating was employed as the diffractive element to enable both beam steering and echo collection. Reflected pulses were compressed by dispersion-compensating fiber, implementing an all-optical DFT for localization. The DFT enabled precise frequency extraction from pulse separation and offered much faster processing than electronic methods. The demonstrated all-optical pulse compression method operates within the same wavelength–angle and time-of-flight localization framework as our previous work, confirming its compatibility with full user localization architectures. This approach offers an efficient, low-latency solution for next-generation indoor OWC localization.

Funding. Engineering and Physical Sciences Research Council (EP/S005625/1); Royal Society (IEC/NSFC/242355).

Disclosures. The authors declare no conflicts of interest.

Data availability. Data underlying the results presented in this paper are not publicly available at this time but may be obtained from the authors upon reasonable request.

REFERENCES

1. H. Weng, W. Wang, Z. Chen, *et al.*, Photonics **11**, 722 (2024).
2. K. Wang, C. Fang, M. O. Ali, *et al.*, Adv. Photon. Res. **6**, 2500015 (2025).
3. Y. Yue and C. Wang, In *Optoelectronics and Communications Conference (OECC)* OSA Technical Digest (Optica Publishing Group 2021), paper JS2B.5.
4. J. Singh, N. Tyagi, S. Singh, *et al.*, IEEE Internet Things J. **11**, 34717 (2024).
5. N. Q. Pham, K. Mekonnen, E. Tangdiongga, *et al.*, IEEE Photon. Technol. Lett. **33**, 545 (2021).
6. S. Chen, W. Li, W. Zheng, *et al.*, Electronics **14**, 994 (2025).
7. Y. Yue, C. K. Mididoddi, N. Jing, *et al.*, IEEE Photon. Technol. Lett. **33**, 1030 (2021).
8. C. Wang, M. Li, and J. Yao, IEEE Photon. Technol. Lett. **22**, 1285 (2010).
9. M. Li and J. Yao, IEEE Photon. Technol. Lett **23**, 1439 (2011).
10. C. Wang and J. Yao, J. Lightwave Technol. **29**, 789 (2011).